SCIENTIFIC REPORTS

OPEN

Remarkably High Hole Mobility Metal-Oxide Thin-Film Transistors

Cheng Wei Shih[1], Albert Chin[1], Chun Fu Lu[2] & Wei Fang Su[2]

Received: 22 August 2017
Accepted: 30 October 2017
Published online: 17 January 2018

High performance p-type thin-film transistor (p-TFT) was realized by a simple process of reactive sputtering from a tin (Sn) target under oxygen ambient, where remarkably high field-effect mobility (μ_{FE}) of 7.6 cm^2/Vs, 140 mV/dec subthreshold slope, and 3×10^4 on-current/off-current were measured. In sharp contrast, the SnO formed by direct sputtering from a SnO target showed much degraded μ_{FE}, because of the limited low process temperature of SnO and sputtering damage. From the first principle quantum-mechanical calculation, the high hole μ_{FE} of SnO p-TFT is due to its considerably unique merit of the small effective mass and single hole band without the heavy hole band. The high performance p-TFTs are the enabling technology for future ultra-low-power complementary-logic circuits on display and three-dimensional brain-mimicking integrated circuits.

The metal-oxide thin-film transistors (TFTs)[1–22] have attracted much attention for next-generation display due to its high mobility in comparison to the silicon-based TFTs, good optical transparency in visible light region, and compatibility with low-temperature processes. To incorporate control integrated circuit (IC) into display and lower the power consumption, high mobility metal-oxide p-type TFT (p-TFT) is required. Such complementary n- and p-TFTs are the needed technology for tens of years since the TFT invention[17–23]. However, most metal-oxide TFTs[1–13] show n-type conduction. Only very few oxides such as Cu_xO[14,18], NiO_x[15,16], and SnO[20] exhibit p-type conduction with a low mobility. Therefore, the development of high mobility metal-oxide p-TFT is crucial to embed low-power complementary logic circuits on display for system-on-panel. Previously, we pioneered very high mobility SnO_2 n-TFTs[10–12]. In this paper, we investigated the device performance and material property of SnO p-TFT with the same Sn material. Using hafnium oxide (HfO_2) as the gate dielectric, the HfO_2/SnO p-TFT has a high field-effect mobility (μ_{FE}) of 7.6 cm^2/Vs, small 140 mV/dec subthreshold slope (*SS*), and 3×10^4 on-current/off-current (I_{ON}/I_{OFF}). From the first principle quantum-mechanical calculation, the SnO is one of the best candidates for p-TFT, due to its smaller hole effective mass and unique merit without heavy hole band. The high device performance, simple process, and low-cost material make SnO the excellent candidate for future p-TFTs.

Results

Figure 1(a) and (b) show the transistor's drain-source current versus drain-source voltage (I_{DS}-V_{DS}), $|I_{DS}|$ versus gate-source voltage ($|I_{DS}|$-V_{GS}) and μ_{FE}-V_{GS} characteristics of the HfO_2/SnO_x p-TFTs, where the SnO_x was formed by reactive sputter from a Sn target. Good device performance was reached at a low V_{DS} of −1.2 V that is vital to lower the switching power of $CV_{DS}^2f/2$, where C and f are the capacitance and operation frequency, respectively. Besides, high hole μ_{FE} of 7.6 cm^2/Vs, a *SS* of 140 mV/dec, and an I_{ON}/I_{OFF} of 3×10^4 were obtained. The device mobility is among the best reported p-TFTs in literature[19,20]. It is important to notice that the device performance is highly related to oxygen content. The μ_{FE} was degraded by an order of magnitude at higher O_2/Ar ratio, where the degraded mobility is related to the increasing SnO_2 content inside the SnO.

The reactive sputtering from a Sn target is the crucial technique to reach high hole mobility. Figure 2(a) and (b) show the device characteristics of HfO_2/SnO_x p-TFTs, where the SnO_x was formed by directly sputtering from a SnO target. A low hole μ_{FE} of 0.83 cm^2/Vs, a poor *SS* of 430 mV/dec, and a small I_{ON}/I_{OFF} of 1.2×10^3 were measured. Even poor μ_{FE} value was measured at annealing temperature higher than 200 °C. The high temperature is needed to anneal out the sputtering damage by energetic ions. But the annealing temperature higher than 200 °C cannot be applied to SnO device, because the SnO will translate to low mobility Sn_3O_4 and SnO_2 at high temperatures[24,25].

We have further performed the material analysis to understand the large device performance difference between sputtering from the Sn and SnO targets. Figure 3(a) shows the structure of fabricated Ni/SnO_x/HfO_2

[1]Department of Electronics Engineering, National Chiao Tung University, Hsinchu, 300, Taiwan. [2]Depatment of Materials Science & Engineering, National Taiwan University, Taipei, 10617, Taiwan. Correspondence and requests for materials should be addressed to A.C. (email: achin@faculty.nctu.edu.tw)

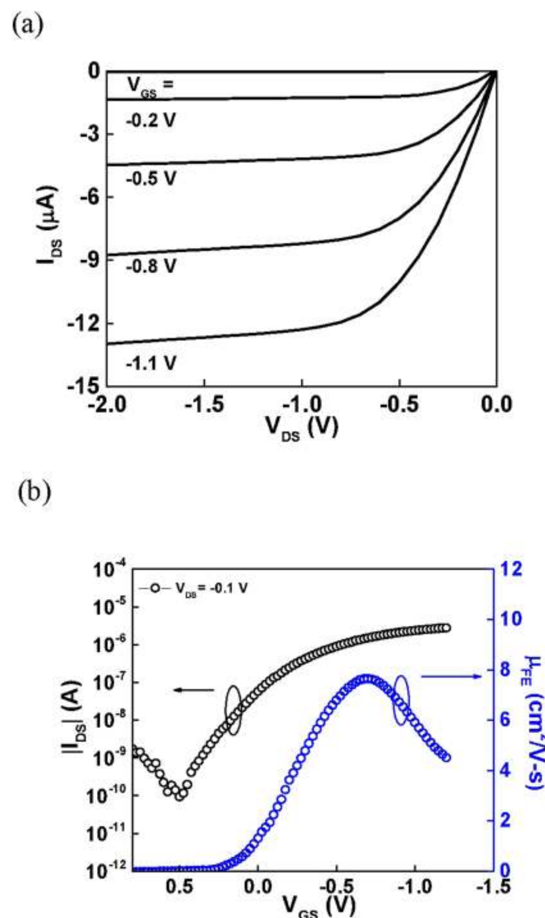

Figure 1. (**a**) I_{DS}-V_{DS} characteristics and (**b**) $|I_{DS}|$-V_{GS} and μ_{FE}-V_{GS} characteristics of Ni/SnO_x/HfO_2/TaN TFTs under an $Ar/O_2 = 1.0$, where the SnO_x was formed by reactive sputter from a Sn target.

device. From the cross-sectional transmission electron microscopy (TEM), the SnO_x active layer on HfO_2 has a thickness of 12 nm. The microscopic structure of SnO_x was analyzed by X-ray diffraction (XRD) as shown in Fig. 3(b). For SnO_x formed by reactive sputtering from a Sn target, a mixture of major tetragonal α-SnO phase and small amount of β-Sn phase is observed that was caused by the incomplete Sn oxidation[26,27]. In contrast, only a pure α-SnO phase was found from the SnO target. The atomic composition of SnO_x in p-TFT are further characterized by X-ray photoelectron spectroscopy (XPS) in Fig. 3(c). The de-convoluted spectra in both cases show a major Sn^{2+} peak with tiny Sn^{4+} and Sn° peaks, although the later ones are smaller for directly sputtered SnO than those from reactive sputtering of a Sn target. Therefore, the SnO_x by sputtering from a SnO target gives better material quality. Nevertheless, the μ_{FE} is significantly lower than that from the reactive Sn target. The potential reason may be related to the sputter damage from the SnO target, which is difficult to be detected by XRD and XPS analysis. Unfortunately such damage cannot be annealed out because of the limited process temperature of SnO, which can react as scattering centers to low the mobility. The other possibility to reach high mobility may be related to the multi-phonon assisted tunneling[28] via small amount of metallic Sn in SnO. This is also associated with the lower off-current in reactive sputtered SnO device than that formed by sputtering from the SnO target. Further theoretical analysis will be required to understand the role of metallic Sn inside SnO. Nevertheless, the metallic Sn is difficult to form by sputtering from the SnO target.

It is crucial to notice that the measured hole μ_{FE} is the highest value among oxide semiconductors. We further perform the first principle quantum-mechanical calculations on SnO and the other potential candidate of Cu_2O (Figures S1 and S2). The structures of both SnO and Cu_2O semiconductors were obtained using local density approximation plus U (LDA + U) method with appropriate U^p and U^d value. The good accuracy is supported by the calculated band structure of Cu_2O; a direct 2.1 eV bandgap and cubic structure were obtained, agreeing well with experiments[14,29,30]. Both light hole and heavy hole bands were found in Cu_2O that are typical for most major semiconductors of Si, Ge, GaAs, InP, InAs etc. Besides, the density of state (DOS) of heavy hole band is considerably higher than that of light hole band to cause the low hole mobility. In sharp contrast, the SnO only has a single hole band, leading to the high hole μ_{FE}. The calculated DOS of SnO and Cu_2O are further shown in Fig. 4. The Cu_2O has much higher DOS than SnO due to its heavy hole bands. For Cu_2O, the d-orbital holes have complex intra-atomic hybridization between d and s, p states that lowers the hole mobility. This is also applied for

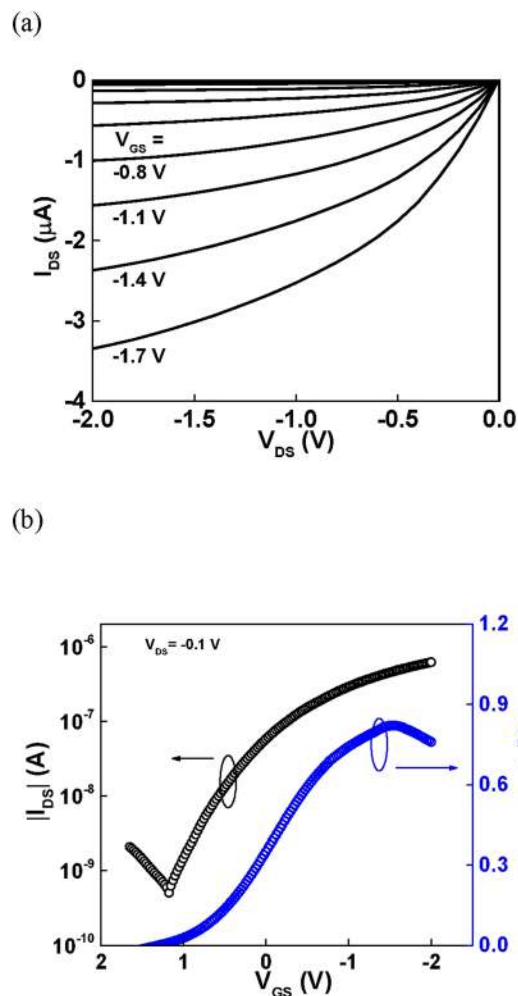

Figure 2. (**a**) I_{DS}-V_{DS} characteristics and (**b**) $|I_{DS}|$-V_{GS} and μ_{FE}-V_{GS} characteristics of Ni/SnO_x/HfO_2/TaN TFTs, where the SnO_x was formed by sputter directly from a SnO target.

Channel Materials	Channel layer thickness (nm)	Gate Insulator Materials	*SS* (V/decade)	μ_{EF} (cm^2/V·s)	I_{ON}/I_{OFF}	Operating Voltage (V)
NiO [15]	30	SiO_2	—	5.2	~10^3	−100
Cu_xO [19]	—	ScO_x	~0.4	0.8	~10^5	−3
SnO [20]	15	SiO_2	0.55	3.3	10^4	−3
SnO [25]	27	SiO_2	0.24	1.4	~10^4	−100
This Work SnO	12	HfO_2	0.14	7.6	3×10^4	−1.2

Table 1. The device performance of various TFTs.

most oxide semiconductors to result in a low hole mobility[31–33]. In sharp contrast, the Sn 5s orbital is occupied and exhibits a s-p coupling with the O 2p ligand orbitals, unlike the p-d interaction of the d^{10} Cu_2O. The delocalized character of the 5s states leads to a strong valence band dispersion and small hole effective masses in SnO (Figure S3). The SnO has much smaller hole effective mass than Cu_2O and other major semiconductors of Si, Ge, GaAs, InP, InGaAs etc. This is the extremely unique merit of SnO p-type transistor to reach high hole mobility.

Table 1 compares the device performance of various TFTs. For p-TFTs, the SnO device has good hole μ_{FE}, *SS*, and I_{ON}/I_{OFF}, which is supported from the small effective mass and single band without heavy hole band. The low V_D operation is important to lower AC power consumption.

In conclusion, record high hole mobility of SnO p-TFT was realized. The superb device performance, simple process, and low-cost material make SnO the excellent candidate for next generation ultra-low power display devices and 3D brain-mimicking IC[10,13].

(a)

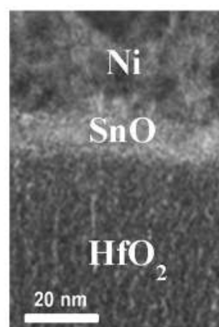

(b)

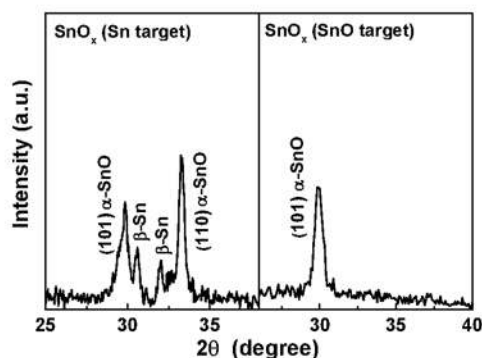

(c)

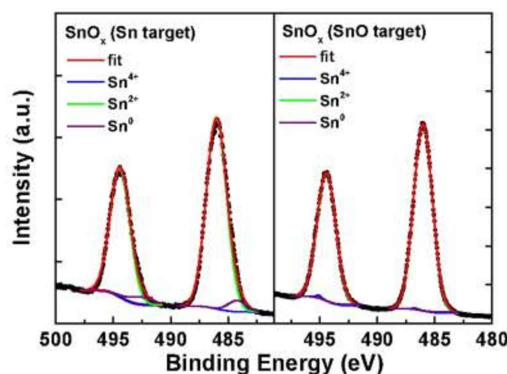

Figure 3. (**a**) TEM, (**b**) XRD, and (**c**) The Sn 3d XPS analysis of SnO_x formed from Sn and SnO targets.

Methods

The bottom-gate TFTs were fabricated on a 500-nm-thick SiO_2 layer over a Si substrate. A 60-nm TaN was first deposited through reactive sputtering and patterned as the bottom gate electrode. Subsequently, gate dielectric of 40-nm-thick high-κ HfO_2 was deposited through physical vapor deposition (PVD) and annealed at 400 °C. Then a 12 nm SnO_x was deposited by sputtering in an Ar/O_2 mixture from a Sn target, under a DC power of 50 W and a pressure of 7.6 mTorr. Alternatively, the SnO_x was deposited by RF sputtering from a SnO_x target in the Ar/O_2 ambient, under a power of 200 W and a pressure of 7.6 mTorr. Then both the SnO films were subjected to post-deposition annealing at 200 °C in N_2 ambient. Finally, the Ni was deposited to form source-drain electrodes. The gate length and width were 50 and 500 μm, respectively. The electrical characteristics of the fabricated devices were measured using an HP4155B parameter analyzer and a probe station. The SnO film was analyzed by transmission electron microscopy (TEM), X-ray diffraction (XRD), and X-ray photoelectron spectroscopy (XPS). The XPS spectra were measured with a PHI 5000 VersaProbe system (ULVAC-PHI, Chigasaki) using a microfocused (100 μm, 25 W) Al X-ray beam. Cross section TEM images of devices were obtained from high

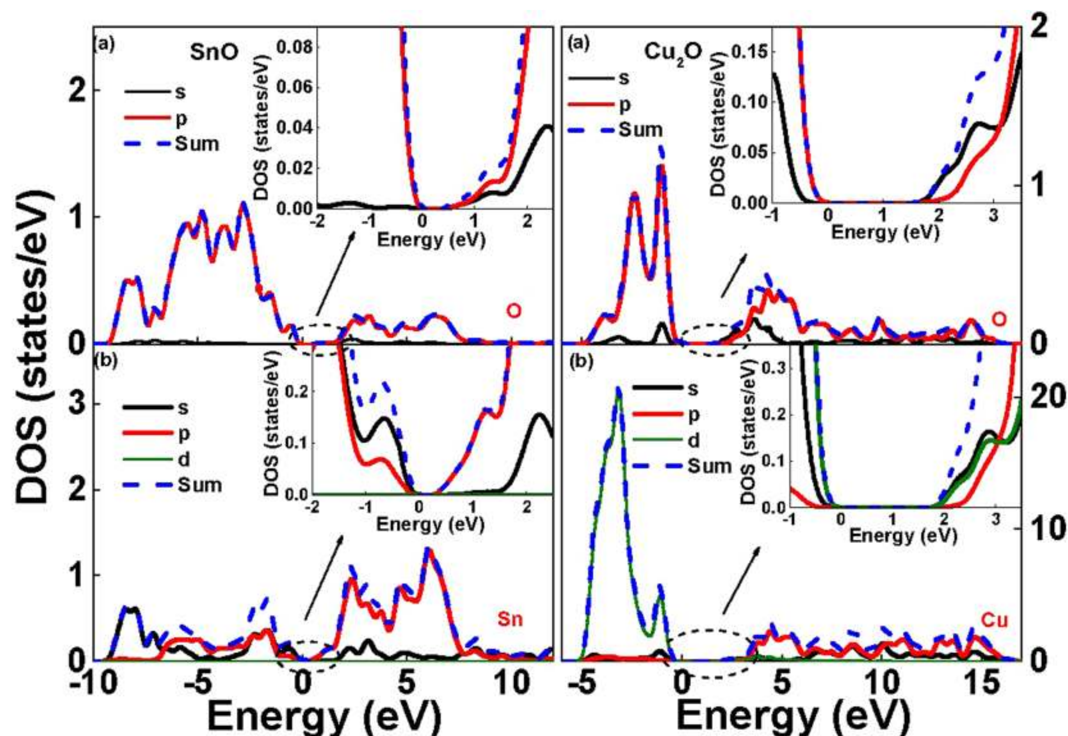

Figure 4. DOS distribution of SnO and Cu_2O, where d and s, p states hybridization is found for Cu_2O.

resolution transmission electron microscope (JEOL 2010F, USA). The first principle quantum-mechanical calculation was applied to compute the theoretical structural and electrical properties of SnO and Cu_2O, using Cambridge Sequential Total Energy Package code (Materials Studio 8.0) with generalized gradient approximation (GGA) and local-density approximations plus Hubbard potential U (LDA + U) method.

References

1. Fortunato, E. M. C. *et al*. Fully transparent ZnO thin-film transistor produced at room temperature. *Adv. Mater.* **17**, 590 (2005).
2. Zan, H. W., Yeh, C. C., Meng, H. F., Tsai, C. C. & Chen, L. H. Achieving high field-effect mobility in amorphous indium-gallium-zinc oxide by capping a strong reduction layer. *Adv. Mater* **24**, 3509 (2012).
3. Nomura, K. *et al*. Thin-film transistor fabricated in single-crystalline transparent oxide semiconductor. *Science* **300**, 1269 (2003).
4. Suresh, A., Wellenius, P. & Muth, J. F. High performance transparent thin film transistors based on indium gallium zinc oxide as the channel material. *IEDM Tech. Dig*. 587 (2007).
5. Kim, S. I. *et al*. High performance oxide thin film transistors with double active layers. *IEDM Tech. Dig*. 73 (2008).
6. Kim, T. S. *et al*. High Performance gallium-zinc oxynitride thin film transistors for next-generation display applications. *IEDM Tech. Dig*. 660 (2013).
7. Lee, E. *et al*. Nanocrystalline ZnON; High mobility and low band gap semiconductor material for high performance switch transistor and image sensor application. *Scientific Reports* **4**, 4948 (2014).
8. Bak, J. Y. *et al*. Origin of degradation phenomenon under drain bias stress for oxide thin film transistors using IGZO and IGO channel layers. *Scientific Reports* **5**, 7884 (2015).
9. Park, J. C. *et al*. High performance amorphous oxide thin film transistors with self-aligned top-gate structure. *IEDM Tech. Dig*. 191 (2009).
10. Shih, C. W., Chin, A., Lu, C. F. & Yi, S. H. Extremely high mobility ultra-thin metal-oxide with ns^2np^2 configuration. *IEDM Tech. Dig*. 145 (2015).
11. Shih, C. W., Chin, A., Lu, C. F. & Su, W. F. Remarkably high mobility ultra-thin-film metal-oxide transistor with strongly overlapped orbitals. *Sci. Rep.* **6**, 19023 (2016).
12. Shih, C. W. & Chin, A. New material transistor with record-high field-effect mobility among wide-band-gap semiconductors. *ACS Appl. Mater. Interfaces* **8**, 19187 (2016).
13. Shih, C. W. & Chin, A. Remarkably High mobility thin-film transistor on flexible substrate by novel passivation material. *Scientific Reports* **7**, 1147 (2017).
14. Pattanasattayavong, P., Thomas, S., Adamopoulos, G., McLachlan, M. A. & Anthopoulos, T. D. P-channel thin-film transistors based on spray-coated Cu_2O films. *Appl. Phys. Lett.* **102**, 163505 (2013).
15. Jiang, J., Wang, X., Zhang, Q., Li, J. & Zhang, X. Thermal oxidation of Ni films for p-type thin-film transistors. *Phys. Chem. Chem. Phys.* **15**, 6875 (2013).
16. Lin, T., Li, X. & Jang, J. High performance p-type NiO_X thin-film transistor by Sn doping. *Appl. Phys. Lett.* **108**, 233503 (2016).
17. Ohshima, H. & Morozumi, S. Future trends for TFT integrated circuits on glass substrates. *IEDM Tech. Dig*. 157 (1989).
18. Oana, Y. Current and future technology of low-temperature poly-Si TFT-LCDs. *J. SID*. 169 (2001).
19. Liu, A. *et al*. Water-induced scandium oxide dielectric for low-operating voltage n- and p-type metal-oxide thin-film transistors. *Adv. Funct. Mater.* **25**, 7180 (2015).
20. Zhong, C. W., Lin, H. C., Liu, K. C. & Huang, T. Y. Improving electrical performances of p-type SnO thin-film transistors using double-gated structure. *IEEE Electron Device Lett.* **36**, 1053 (2015).
21. Liang, L. Y. *et al*. Ambipolar inverters using SnO thin-film transistors with balanced electron and hole mobilities. *Appl. Phys. Lett.* **100**, 263502 (2012).

22. Nomura, K., Kamiya, T. & Hosono, H. Ambipolar oxide thin-film transistor. *Adv. Mater.* **23**, 3431 (2011).
23. Wang, H. *et al*. Large-scale 2D electronics based on single-layer MoS_2 grown by chemical vapor deposition. *IEDM Tech. Dig.* 88 (2012).
24. Hosono, H., Ogo, Y., Yanagi, H. & Kamiya, T. Bipolar conduction in SnO thin films. *Electrochem. Solid-State Lett.* **14**, H13 (2011).
25. Li, Y. *et al*. Extremely sensitive dependence of SnO_x film properties on sputtering power. *Scientific Reports* **6**, 36183 (2016).
26. Luo, H., Liang, L. Y., Cao, H. T., Liu, Z. M. & Zhuge, F. Structural, chemical, optical, and electrical evolution of SnO_x films deposited by reactive rf magnetron sputtering. *ACS Appl. Mater. Interfaces* **4**, 5673 (2012).
27. Wang, Z. *et al*. Transparent SnO–SnO_2 p–n junction diodes for electronic and sensing applications. *Adv. Mater. Interfaces* **2**, 1500374 (2015).
28. Shaposhnikov, A. V., Perevalov, T. V., Gritsenko, V. A., Cheng, C. H. & Chin, A. Mechanism of GeO_2 resistive switching based on the multi-phonon assisted tunneling between traps. *Appl. Phys. Lett.* **100**, 243506 (2012).
29. Nakano, Y., Saeki, S. & Morikawa, T. Optical bandgap widening of p-type Cu_2O films by nitrogen doping. *Appl. Phys. Lett.* **94**, 022111 (2009).
30. Figueiredo, V. *et al*. p-Type Cu_xO films deposited at room temperature for thin-film transistors. *J. Display Technol.* **8**, 1 (2012).
31. Meng, J., Jena, P. & Vail, J. M. Hole trapping in $Li_xNi_{1-x}O$. *J. Phys.: Condens. Matter* **2**, 10371 (1990).
32. Kamiya, T. & Hosono, H. Material characteristics and applications of transparent amorphous oxide semiconductors. *NPG Asia Mater.* **2**, 15 (2010).
33. Granato, D. B., Caraveo-Frescas, J. A., Alshareef, H. N. & Schwingenschlogl, U. Enhancement of p-type mobility in tin monoxide by native defects. *Appl. Phys. Lett.* **102**, 212105 (2013).

Acknowledgements
The publication of this paper was supported in part by Ministry of Science and Technology of Taiwan. We would like to thank the computing time support from National Taiwan University of Science & Technology and National Center for High-performance Computing. The results of this research have important financial interests for both Display and ultra-low power 3D IC.

Author Contributions
C.W. Shih did the experiments; Albert Chin wrote the main manuscript text; C. Fu Lu and W.F. Su did the quantum-mechanical calculations. All authors reviewed the manuscript.

Additional Information
Supplementary information accompanies this paper at https://doi.org/10.1038/s41598-017-17066-x.

Competing Interests: The authors declare that they have no competing interests.

Publisher's note: Springer Nature remains neutral with regard to jurisdictional claims in published maps and institutional affiliations.

Open Access This article is licensed under a Creative Commons Attribution 4.0 International License, which permits use, sharing, adaptation, distribution and reproduction in any medium or format, as long as you give appropriate credit to the original author(s) and the source, provide a link to the Creative Commons license, and indicate if changes were made. The images or other third party material in this article are included in the article's Creative Commons license, unless indicated otherwise in a credit line to the material. If material is not included in the article's Creative Commons license and your intended use is not permitted by statutory regulation or exceeds the permitted use, you will need to obtain permission directly from the copyright holder. To view a copy of this license, visit http://creativecommons.org/licenses/by/4.0/.

© The Author(s) 2018